MOX–Report No. 34/2011

A spectral collocation method for the one dimensional shallow water equations on semi-infinite domains

Benacchio, T.; Bonaventura, L.

MOX, Dipartimento di Matematica "F. Brioschi"
Politecnico di Milano, Via Bonardi 9 - 20133 Milano (Italy)

mox@mate.polimi.it http://mox.polimi.it

A spectral collocation method for the one dimensional shallow water equations on semi–infinite domains

Tommaso Benacchio[♯ *], Luca Bonaventura[♯]

July 27, 2011

[♯]MOX – Modelling and Scientific Computing,
Dipartimento di Matematica "F. Brioschi", Politecnico di Milano
Via Bonardi 9, 20133 Milano, Italy
benacchio@math.fu-berlin.de
luca.bonaventura@polimi.it

Keywords: Laguerre functions, spectral methods, open boundary conditions, semi-implicit schemes, shallow water equations.

AMS Subject Classification: 42C10, 65M70, 65Z05, 76M22, 86A10

Abstract

We introduce a spectral collocation method for the discretization of the shallow water equations on a one dimensional semi-infinite domain, employing suitably rescaled Laguerre basis functions to obtain an accurate description of the solutions on finite regions of arbitrary size. The time discretization is based on a semi-implicit, semi-Lagrangian approach that allows to handle the highly inhomogeneous node distribution without loss of efficiency. The method is first validated on standard test cases and then applied to the implementation of absorbing open boundary conditions by coupling the semi-infinite domain to a finite size domain on which the same equations are discretized by standard finite volume methods. Numerical experiments show that the proposed approach does not produce significant spurious reflections at the interface between the finite and infinite domain, thus providing a reliable tool for absorbing boundary conditions.

[*]Now at: FB Mathematik und Informatik, Freie Universität Berlin, Arnimallee 6, 14195 Berlin, Germany.

1 Introduction

In this paper we introduce a pseudo–spectral method based on Laguerre functions expansions for the approximation of wave propagation problems on semi–infinite domains.

The purpose of this development is twofold. On one hand, in many environmental applications it is of interest to consider computational domains that span over very different length scales. In climate modelling, increasing attention has been devoted to stratospheric phenomena, see e.g. [12, 15], which requires to extend vertically the typical computational domain of standard climate models by a substantial amount. In an early attempt to use Laguerre basis functions for the vertical discretization of the equations of atmospheric flow, Francis [10] reported that they "entail a computational penalty that more than compensates for the advantages gained by using analytic vertical representation". It is therefore of interest to assess whether, with the theoretical and computational resources currently at our disposal, spectral or pseudo–spectral approaches can be used to devise accurate and efficient discretizations for domains with arbitrarily large length scales. We do so considering as model equations the one dimensional shallow water equations, that provide a standard model for wave propagation problems. Regarding the numerical discretization, a semi–implicit, semi–Lagrangian approach, see e.g. [6, 29, 33], has been chosen because of its well–known efficiency and accuracy features and because a large number of environmental models use these time discretization techniques.

On the other hand, for computational reasons it is common to restrict the simulation to a bounded domain of interest and to apply some kind of open boundary condition to let waves propagate out of the computational domain. Since conventional boundary conditions such as rigid lids or constant pressure surfaces entail total reflection of wave energy, two classical approaches to this problem, radiative boundary conditions and absorbing (or sponge) layers, have been extensively applied in the last three decades to atmospheric models for numerical weather prediction and climate, see e.g. the reviews [14, 28]. In this respect, the other main goal of this work is the use of Laguerre spectral methods for the implementation of absorbing layer boundary conditions, by coupling discretizations on domains of finite size to Laguerre spectral methods. If a relatively small number of nodes is employed, an efficient approach to absorbing boundary conditions can be achieved, that allows to account for large absorbing regions at a relatively low computational cost. The coupling approach is based on imposing continuity of the mass fluxes at the interface between the bounded and the unbounded domain. The same idea can be in principle extended to couple the Laguerre spectral method to an arbitrary discretization on the bounded domain. In this first attempt, an explicit finite volume discretization has been considered for the finite size domain. Numerical tests show that spurious reflections due to the proposed coupling approach have very small amplitude and allow to use the proposed method, at least for environmental applications, with no substantial loss of accuracy with respect to single domain discretizations.

The rest of the paper is organized as follows. Section 2 contains a review

of the main results concerning polynomial approximations and interpolation on semi–infinite domains by scaled Laguerre functions. In section 3 a spectral collocation method based on scaled Laguerre functions is introduced, in order to show that the shallow water equations can be approximated accurately and efficiently on semi–infinite domains by extensions of semi–implicit, semi–Lagrangian methods that are customary in many environmental applications. Different numerical approaches to the approximation of open boundary conditions are reviewed and discussed in section 4, with special attention to absorbing boundary conditions. The semi–infinite discretization is then coupled to a finite volume discretization of the shallow water equations on a finite size domain, as detailed in section 5. Section 6 contains the results of a number of numerical tests. A first goal of these tests is to validate the pseudo–spectral, semi–implicit and semi–Lagrangian discretization approach on semi–infinite domains as an independent tool. The coupling approach is then validated, by comparison of the coupled finite volume/pseudo–spectral model results to those of reference runs of the finite volume model on a single domain. Finally, absorbing boundary conditions are validated, as implemented in the context of the coupled finite volume/pseudo–spectral model. Numerical simulations show that a reasonable number of spectral base functions is sufficient to reach the accuracy necessary for practical implementations of open boundary conditions, along with an accurate treatment of the solution behaviour at infinity. Some conclusions on the present work are drawn in section 7, where the perspectives for further development of this approach are also discussed.

2 Laguerre polynomials and functions on the half line

Laguerre polynomials and functions are a classical tool for polynomial approximations on semi–infinite domains, see e.g. [4]. In–depth analysis has been carried out to assess the efficiency and accuracy properties of these systems in spectral discretizations of initial and boundary–value problems (see [30, 35] and the review in [32]). More recently, the introduction of scaled Laguerre polynomials and functions has enabled to approximate solutions with different asymptotic behaviours [34]. We recall here the main results for scaled Laguerre functions. A more extensive review of the results on approximation, quadrature rules, interpolation and spectral differentiation can be found in [2].

Let $\omega_\beta(x) = \mathrm{e}^{-\beta x}$, $\beta > 0$, be a weight function on $\mathbb{R}^+$. Scaled Laguerre polynomials (shortly, SLPs) $\left\{\mathscr{L}_n^{(\beta)}\right\}_{n\in\mathbb{N}}$ are a system of orthogonal polynomials in $L^2_{\omega_\beta}(\mathbb{R}^+)$, that is:

$$\int_0^{+\infty} \mathscr{L}_n^{(\beta)}(x)\mathscr{L}_m^{(\beta)}(x)\omega_\beta(x)dx = \frac{1}{\beta}\delta_{nm}, \qquad n, m \in \mathbb{N}.$$

Scaled Laguerre functions (SLFs) $\left\{\widehat{\mathscr{L}_n}^{(\beta)}\right\}_{n\in\mathbb{N}}$ are defined by:

$$\widehat{\mathscr{L}_n}^{(\beta)}(x) = \mathrm{e}^{-\beta x/2}\mathscr{L}_n^{(\beta)}(x).$$

SLFs are orthogonal in $L^2(\mathbb{R}^+)$, that is:

$$\int_0^{+\infty} \widehat{\mathscr{L}}_n^{(\beta)}(x)\widehat{\mathscr{L}}_m^{(\beta)}(x)\omega_\beta(x)dx = \frac{1}{\beta}\delta_{nm}, \qquad n,m \in \mathbb{N}.$$

Since $\left\{\widehat{\mathscr{L}}_n^{(\beta)}\right\}_{n\in\mathbb{N}}$ is a complete orthogonal basis of $L^2(\mathbb{R}^+)$, any function can be expanded in series of SLFs, namely:

$$Su = \sum_{k=0}^{\infty} \widehat{u}_k \widehat{\mathscr{L}}_k^{(\beta)}, \qquad S_N u = \sum_{k=0}^{N} \widehat{u}_k \widehat{\mathscr{L}}_k^{(\beta)},$$
$$\widehat{u}_k = \beta\left(u, \widehat{\mathscr{L}}_k^{(\beta)}\right),$$

where $S_N u$ and $\widehat{u}_k$ are the N–th order truncated of Su and the k–th Fourier–Laguerre coefficient, and $(\cdot,\cdot)$ is the dot product in $L^2(\mathbb{R}^+)$. We remark that in our case we will set $\beta = \dfrac{1}{L}$, where L stands for a typical length scale in the application of interest. If semi–infinite domains are considered, one will have $\beta \ll 1$.

Since we focus on problems on semi–infinite domains, we use Gauss–Radau quadrature formulas (see e.g. [27, 31]), whose nodes include the left endpoint of the domain. Referring to integrations on the half line $I = [0, +\infty)$, the scaled Gauss–Laguerre–Radau quadrature rule based on SLFs reads as follows:

$$\int_0^{+\infty} p(x)dx = \sum_{j=0}^{N} p\left(x_j^{(\beta)}\right)\widehat{\omega}_j^{(\beta)} \qquad \forall p \in \widehat{\mathbb{P}}_{2N}^{(\beta)},$$

where:

$x_0^{(\beta)} = 0$, $\left\{x_j^{(\beta)}\right\}_{j=1}^{N}$ are the zeros of $\partial_x \mathscr{L}_{N+1}^{(\beta)}(x)$;

$$\omega_j^{(\beta)} = \frac{\mathrm{e}^{\beta x_j^{(\beta)}}}{\beta(N+1)\left[\mathscr{L}_N^{(\beta)}(x_j^{(\beta)})\right]^2}, \quad 0 \le j \le N,$$

and:

$$\widehat{\mathbb{P}}_N^{(\beta)}(I) = \left\{u \mid u = v\mathrm{e}^{-\beta x/2}, v \in \mathbb{P}_N\right\},$$

where $\mathbb{P}_N(I)$ is the space of polynomials of degree at most N in I. As for the efficient computation of nodes and weights, see the discussion in [2].

Next, we define the interpolation operator $\widehat{I}_N^{(\beta)} : C([0,+\infty)) \to \widehat{\mathbb{P}}_N^{(\beta)}$ by:

$$\widehat{I}_N^{(\beta)} u(x) = \sum_{n=0}^{N} \widetilde{u}_n^{(\beta)} \widehat{\mathscr{L}}_n^{(\beta)}(x) \in \widehat{\mathbb{P}}_N^{(\beta)},$$

the coefficients $\left\{\widetilde{u}_n^{(\beta)}\right\}_{n=0}^{N}$ being determined by the *forward discrete transform*:

$$\widetilde{u}_n^{(\beta)} = \sum_{j=0}^{N} u\left(x_j^{(\beta)}\right) \widehat{\mathscr{L}}_n^{(\beta)}\left(x_j^{(\beta)}\right) \widehat{\omega}_j^{(\beta)} \quad 0 \le j \le N.$$

Results on convergence of the interpolation error can be found in [34].

The definition of $\widehat{I}_N^{(\beta)}u(x)$ given above enables also to define a discrete derivative of u, using the analytical derivative of the interpolating polynomial, that is, see [31]:

$$\mathbf{u}^{(m)} = \widehat{D}_\beta^m \mathbf{u}, \qquad m \geq 1,$$

where:

$$\widehat{D}_\beta = \left[\left(\widehat{d}_\beta\right)_{ij}\right]_{i,j=0,\ldots,N} = \left[\left(\widehat{h}_\beta\right)_j'\left(x_i^{(\beta)}\right)\right]_{i,j=0,\ldots,N}, \tag{1}$$

$$\mathbf{u}^{(m)} = \left(u^{(m)}(x_0), u^{(m)}(x_1), \ldots, u^{(m)}(x_N)\right)^T, \quad \mathbf{u} = \mathbf{u}^{(0)},$$

$\left\{(\widehat{h}_\beta)_j(x)\right\}_{j=0}^N$ being the Lagrange interpolation functions relative to the nodes $\left\{x_j^{(\beta)}\right\}_{j=0}^N$, defined by the interpolation conditions:

$$\left(\widehat{h}_\beta\right)_j \in \widehat{\mathbb{P}}_N^{(\beta)}, \ \left(\widehat{h}_\beta\right)_j\left(x_i^{(\beta)}\right) = \delta_{ij} \quad 0 \leq i,j \leq N.$$

Lagrange interpolation functions can be easily computed from Lagrange interpolation polynomials relative to $\left\{x_j^{(\beta)}\right\}_{j=0}^N$ by:

$$\left(\widehat{h}_\beta\right)_j(x) = \frac{\mathrm{e}^{-\beta x/2}}{\mathrm{e}^{-\beta x_j^{(\beta)}/2}}\left(h_\beta\right)_j(x).$$

In particular, the derivative reads:

$$\left(\widehat{h}_\beta\right)_j'\left(x_i^{(\beta)}\right) = \frac{\mathrm{e}^{-\beta x_i^{(\beta)}/2}}{\mathrm{e}^{-\beta x_j^{(\beta)}/2}}\left[\left(\widehat{h}_\beta\right)_j'\left(x_i^{(\beta)}\right) - \frac{\beta}{2}\delta_{ij}\right].$$

Therefore, the entries of the differentiation matrix (1) have the following form:

$$\left(\widehat{d}_\beta\right)_{ij} = \begin{cases} \dfrac{\widehat{\mathscr{L}}_{N+1}^{(\beta)}\left(x_i^{(\beta)}\right)}{\left(x_i^{(\beta)} - x_j^{(\beta)}\right)\widehat{\mathscr{L}}_{N+1}^{(\beta)}\left(x_j^{(\beta)}\right)} & \text{if } i \neq j \\ 0 & \text{if } i = j \neq 0 \\ -\beta\dfrac{N+1}{2} & \text{if } i = j = 0 \end{cases}$$

3 A semi-implicit, semi-Lagrangian spectral collocation method for the shallow water equations on semi-infinite domains

The shallow water equations describe waves arising from perturbations of the free surface of a shallow layer of fluid within a constant gravitational

field, see e.g. [6, 7]. In the spatial and temporal domain $\mathbb{R}^+ \times \mathbb{R}^+$ they read:

$$\begin{cases} \dfrac{\partial \eta}{\partial t} + \dfrac{\partial (Hu)}{\partial x} + \gamma \eta = 0 & x \in \mathbb{R}^+, t > 0 \quad (2a) \\ \dfrac{\partial u}{\partial t} + u \dfrac{\partial u}{\partial x} + g \dfrac{\partial \eta}{\partial x} + \gamma u = 0 & x \in \mathbb{R}^+, t > 0 \quad (2b) \\ \dfrac{\partial (Hu)}{\partial x}(0,t) = f(t) & (2c) \\ \eta(x,0) = \eta_0(x) & (2d) \\ u(x,0) = u_0(x) & (2e) \end{cases}$$

together with initial conditions and, e.g., Neumann boundary conditions on the fluid discharge at the left endpoint. Other boundary conditions could also be considered. Above, η represents the water surface elevation measured from the undisturbed water surface $z = 0$, $H = z_b + \eta$ the total water depth, and z_b the water depth measured from the undisturbed water surface, see figure 1. Moreover, we have already taken into account a damping reaction term in both equations, that will be used to represent the absorbing layer.

As for the continuity equation (2a), we discretize it with θ–method in

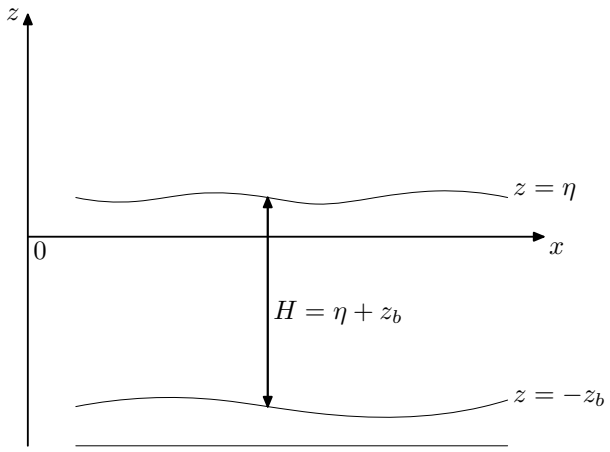

Figure 1: Vertical section of free–surface flow.

time and spectral collocation in space. On the other hand, the advective nonlinearity in the momentum equation (2b) is discretized by adopting a semi–Lagrangian approach (for a review see e.g. [33]). The value of the solution at time $n+1$ at the mesh points is expressed in terms of the solution values at time n at those points that within a single step are transported by the flow onto the computational mesh, i.e.:

$$\frac{\partial u}{\partial t} + u \frac{\partial u}{\partial x} = \frac{\mathrm{D}u}{\mathrm{D}t} \approx \frac{u^{n+1} - u_*^n}{\Delta t},$$

where $u_*^n = u^n(x_*)$ and x_* denotes the *foot* of the characteristic, that can be determined by numerical solution of the equation:

$$\frac{dx}{dt} = u^n(x)$$

backward in time with initial data equal to the mesh nodes. This equation is solved by a simple forward Euler method combined with a substepping approach (see e.g. [6]), while the the velocity values at the point x_* can be retrieved for instance by cubic interpolation, that is:

$$(u_*^n)_i \approx \begin{cases} \displaystyle\sum_{k=i-2}^{i+1} u\left(x_k^{(\beta)}\right) \prod_{\substack{j=i-2 \\ j\neq k}}^{i+1} \frac{x_* - x_j^{(\beta)}}{x_k^{(\beta)} - x_j^{(\beta)}} & \text{if } u_i^n \geq 0 \\ \displaystyle\sum_{k=i-1}^{i+2} u\left(x_k^{(\beta)}\right) \prod_{\substack{j=i-1 \\ j\neq k}}^{i+2} \frac{x_* - x_j^{(\beta)}}{x_k^{(\beta)} - x_j^{(\beta)}} & \text{if } u_i^n < 0 \end{cases}$$

The total depth variable H in the mass flux expression (2a) is treated explicitly, which amounts to a linearization in time.

With a semi–Lagrangian discretization of the material derivative in the momentum equation, the θ–method in time, spectral collocation in space discretization of the system (2a–2e) is:

$$\begin{cases} \left(\dfrac{\eta_N^{n+1} - \eta_N^n}{\Delta t} + \theta \dfrac{\partial}{\partial x}\left(H_N^n u_N^{n+1}\right) + (1-\theta)\dfrac{\partial}{\partial x}\left(H_N^n u_N^n\right) + \gamma \eta_N^{n+1}\right)\left(x_j^{(\beta)}\right) = 0 \\ \left(\dfrac{u_N^{n+1} - (u_N^n)_*}{\Delta t} + g\theta \dfrac{\partial \eta_N^{n+1}}{\partial x} + g(1-\theta)\dfrac{\partial \eta_N^n}{\partial x} + \gamma u_N^{n+1}\right)\left(x_j^{(\beta)}\right) = 0 \\ \dfrac{\partial H_N^n u_N^{n+1}}{\partial x}(x_0^{(\beta)}) = f^{n+1} \\ \eta_N^0 = \eta_{0,N} \in \widehat{\mathbb{P}}_N^{(\beta)} \\ u_N^0 = u_{0,N} \in \widehat{\mathbb{P}}_N^{(\beta)} \end{cases}$$

the first two equations holding for any $j = 1, \ldots, N$. As seen above, if a function $u(x)$ is identified by the vector containing its values in the scaled Gauss–Laguerre-Radau collocation nodes, i.e. $\mathbf{u} = \left[u\left(x_j^{(\beta)}\right)\right]_{j=0}^N$, the derivative of $u(x)$ with respect to x is approximated by the vector obtained multiplying $\mathbf{u}$ by the pseudo–spectral differentiation matrix, that is $\mathbf{u}' = \widehat{D}_\beta \mathbf{u}$, where, dropping from now on the hat on D_β:

$$(D_\beta)_{ij} = \left(\widehat{h}_\beta\right)_j'\left(x_i^{(\beta)}\right) \qquad i, j = 0, \ldots, N.$$

Therefore:

$$u'(x_i) = \sum_{j=1}^{N} (\widehat{h}_\beta)_j'(x_i) u\left(x_j\right) \quad i = 1, \ldots, N,$$

which can be expressed in matrix notation as $\widehat{\mathbf{u}}' = (D_\beta)_N \widehat{\mathbf{u}}$, where $\mathbf{u}$ and the matrix D_β are split in the following way:

$$\mathbf{u} = \left[\begin{array}{c} u_0 \\ \hline \\ \widehat{\mathbf{u}} \\ \\ \end{array}\right], \qquad D_\beta = \left[\begin{array}{c|c} (D_\beta)_{00} & \breve{\mathbf{d}}_\beta \\ \hline \\ \widehat{\mathbf{d}}_\beta & (D_\beta)_N \\ \\ \end{array}\right].$$

Moreover, the boundary condition reads collocationwise as:

$$(d_\beta)^0 \underline{\mathbf{H}}_N^n \mathbf{u}_N^{n+1} = \left[(D_\beta)_{00} \left(H_N^n u_N^{n+1} \right)_0 + \breve{\mathbf{d}}_\beta \left(\underline{\widehat{\mathbf{H}}}_N^n \widehat{\mathbf{u}}_N^{n+1} \right) \right] = f^{n+1}, \qquad (3)$$

where $\underline{\widehat{\mathbf{H}}}_N^n = \text{diag}\left\{ \left[(H_N^n)_i \right]_{i=1}^N \right\}$,

$$\underline{\mathbf{H}}_N^n = \left[\begin{array}{c|ccc} (H_N^n)_0 & 0 & \cdots & 0 \\ \hline 0 & & & \\ \vdots & & \underline{\widehat{\mathbf{H}}}_N^n & \\ 0 & & & \end{array} \right].$$

and $(d_\beta)^0$ denotes the first row of the matrix D_β. These discrete boundary conditions imply that:

$$\begin{aligned} (1 + \gamma_0 \Delta t) \left(\eta_N^{n+1} \right)_0 &= (\eta_N^n)_0 - \Delta t \left[\theta f^{n+1} + (1-\theta) f^n \right] \\ (1 + \gamma_0 \Delta t) \left(u_N^{n+1} \right)_0 &= (u_N^n)_0 - g\Delta t\theta \left[(D_\beta)_{00} \left(\eta_N^{n+1} \right)_0 + \breve{\mathbf{d}}_\beta \widehat{\boldsymbol{\eta}}_N^{n+1} \right] \\ &\quad - g\Delta t(1-\theta) \left[(D_\beta)_{00} (\eta_N^n)_0 + \breve{\mathbf{d}}_\beta \widehat{\boldsymbol{\eta}}_N^n \right], \end{aligned}$$

where $\gamma_0 = \gamma(x_0^{(\beta)})$. Furthermore, setting:

$$\Gamma = \text{diag}\left\{ \left[\gamma(x_i^{(\beta)}) \right]_{i=1}^N \right\}, \; I_\Gamma = I_N + \Delta t \Gamma,$$

the discrete equations for the internal nodes read:

$$\left\{ \begin{array}{l} I_\Gamma \widehat{\mathbf{u}}_N^{n+1} = (\widehat{\mathbf{u}}_N^n)_* - g\Delta t\theta \left[(D_\beta)_N \widehat{\boldsymbol{\eta}}_N^{n+1} + \widehat{\mathbf{d}}_\beta \left(\eta_N^{n+1} \right)_0 \right] \\ \qquad\qquad - g\Delta t (1-\theta) \left[(D_\beta)_N \widehat{\boldsymbol{\eta}}_N^n + \widehat{\mathbf{d}}_\beta (\eta_N^n)_0 \right] \\ I_\Gamma \widehat{\boldsymbol{\eta}}_N^{n+1} = \widehat{\boldsymbol{\eta}}_N^n - \theta\Delta t \left[(D_\beta)_N \widehat{\mathbf{H}}_N^n \widehat{\mathbf{u}}_N^{n+1} + \widehat{\mathbf{d}}_\beta \left(H_N^n u_N^{n+1} \right)_0 \right] \\ \qquad\qquad - (1-\theta) \Delta t \left[(D_\beta)_N \widehat{\mathbf{H}}_N^n \widehat{\mathbf{u}}_N^n + \widehat{\mathbf{d}}_\beta (H_N^n u_N^n)_0 \right] \end{array} \right. \qquad (4)$$

where $(\widehat{\mathbf{u}}_N^n)_* = \left\{ \left[(u_N^n)_* \right]_i \right\}_{i=1,\ldots,N}$.
Replacing $\widehat{\mathbf{u}}_N^{n+1}$, $(\eta_N^{n+1})_0$ and $(u_N^{n+1})_0$ in the second equation one obtains, for the elevation at the internal nodes:

$$\begin{aligned} I_\Gamma \widehat{\boldsymbol{\eta}}_N^{n+1} &= \widehat{\boldsymbol{\eta}}_N^n \\ &\quad - \theta\Delta t \Bigg\{ (D_\beta)_N \widehat{\mathbf{H}}_N^n I_\Gamma^{-1} \left\{ (\widehat{\mathbf{u}}_N^n)_* - g\Delta t\theta (D\eta)_N^{n+1} - g\Delta t (1-\theta) (D\eta)_N^n \right\} \\ &\quad + \widehat{\mathbf{d}}_\beta \frac{(H_N^n)_0}{1 + \gamma_0 \Delta t} \left\{ (u_N^n)_0 - g\Delta t\theta (D\eta)_0^{n+1} - g\Delta t(1-\theta) (D\eta)_0^n \right\} \Bigg\} \\ &\quad - (1-\theta) \Delta t \left[(D_\beta)_N \widehat{\mathbf{H}}_N^n \widehat{\mathbf{u}}_N^n + \widehat{\mathbf{d}}_\beta (H_N^n u_N^n)_0 \right], \end{aligned}$$

where:

$$(D\eta)_N^n = (D_\beta)_N \widehat{\boldsymbol{\eta}}_N^n + \widehat{\mathbf{d}}_\beta (\eta_N^n)_0, \quad (D\eta)_0^n = (D_\beta)_{00} (\eta_N^n)_0 + \breve{\mathbf{d}}_\beta \widehat{\boldsymbol{\eta}}_N^n.$$

After further reductions, the linear system for the elevation internal nodes reads:

$$\begin{aligned}\left\{I_\Gamma - \theta^2 g\Delta t^2 G\right\}\widehat{\boldsymbol{\eta}}_N^{n+1} = &\left\{I_N + \theta(1-\theta)g\Delta t^2 G\right\}\widehat{\boldsymbol{\eta}}_N^n \\ &- \theta\Delta t\,(D_\beta)_N\,\widehat{\mathbf{H}}_N^n I_\Gamma^{-1}\,(\widehat{\mathbf{u}}_N^n)_* + \theta^2 g\Delta t^2\left(\eta_N^{n+1}\right)_0 G_0 \\ &- (1-\theta)\Delta t\,(D_\beta)_N\,\widehat{\mathbf{H}}_N^n\widehat{\mathbf{u}}_N^n \\ &- \Delta t\,(H_N^n)_0\,(u_N^n)_0\,\widehat{\mathbf{d}}_\beta\left(\frac{1+(1-\theta)\gamma_0\Delta t}{1+\gamma_0\Delta t}\right) \\ &+ \theta(1-\theta)g\Delta t^2\,(\eta_N^n)_0\,G_0,\end{aligned} \tag{5}$$

where:

$$G = (D_\beta)_N\,\widehat{\mathbf{H}}_N^n I_\Gamma^{-1}(D_\beta)_N + \frac{(H_N^n)_0}{1+\gamma_0\Delta t}\widehat{\mathbf{d}}_\beta\check{\mathbf{d}}_\beta,$$

$$G_0 = (D_\beta)_N\,\widehat{\mathbf{H}}_N^n I_\Gamma^{-1}\widehat{\mathbf{d}}_\beta + \frac{(H_N^n)_0}{1+\gamma_0\Delta t}\,(D_\beta)_{00}\,\widehat{\mathbf{d}}_\beta.$$

Replacing this expression in the equation for the velocity in (4) gives the solution of the problem at time $n+1$.

4 Open boundary conditions

The problem of open boundary conditions arises whenever wave propagation in unbounded domains has to be modeled. If there is no physical boundary on which boundary conditions can be imposed, one must introduce an artificial boundary $\mathcal{B}$ to encompass the finite region of interest and separate it from the external space. However, as the artificial boundary has no physical counterpart, it must be transparent to the passage of waves propagating in either direction, and no spurious phenomena such as reflection of outgoing waves into the finite computational domain should occur. Referring for example to atmospheric modelling, outgoing waves reflected by the top boundaries can spread to the region of interest and corrupt the numerical solution, see e.g. [23]. Therefore, an accurate analytical and numerical design of the boundary conditions on $\mathcal{B}$ has to be developed. Critical issues in this context involve stability, accuracy, efficiency and ease of implementation of the numerical method approximating the problem in the unbounded domain (for a review see e.g. [14]).

Early suggestions for boundary conditions at the artificial "ceiling" in atmospheric models include setting the vertical velocity to zero at some finite height or, in a pressure coordinate, at $p = 0$ (infinite height). However, both solutions entail total energy reflection or lead to ill–posed formulations (see [28]). Thus, it is in this context that the two most popular approaches to the problem, *radiation boundary conditions* and *absorbing/sponge layers*, have been developed. The basic idea of the *radiation* or *characteristic* boundary conditions (see [9, 16]) is that disturbances propagate across $\mathcal{B}$ as waves that can be described by a simplification of the full model dynamics (see also [18]). On the other hand, *relaxation methods* extend the computational domain to allow disturbances to leave and penetrate into a

limited region (the absorbing layer) where they can be damped by viscous or reaction terms towards the external solution, see e.g. [8, 19, 20]. If the external solution is zero, this approach amounts to introduce a damping term in the layer (see also [17]).

The choice of the relaxation coefficient is a trade–off between the aim to damp efficiently outgoing perturbances on one side and limited spatial resolution, which does not allow for high spatial variations of wave amplitude, on the other. Various functional forms for the parameters have been tested but, as pointed out in [24], the choice of these coefficients and the thickness of the layer have been often directed by empirical criteria. Moreover, a major drawback of this approach is its high computational cost, as considerable effort must be put into simulation of modified equations outside the area of interest, see [14]. Advanced versions of sponge layer formulations have also been developed (see e.g. [25]), leading to *perfectly matched layers*, which split variables into contributions parallel and perpendicular to the boundary, introducing parallel and perpendicular velocity damping coefficients.

A different approach to the problem is given by the use of infinite elements, that have been widely employed in numerical models of wave propagation phenomena from scattering or radiating objects, see e.g. [1, 11]. Similar to finite element, infinite element formulations are local, but their shape functions are chosen to mimic the asymptotic behaviour of the solution at infinity. A clear advantage of such discretizations is the sparseness of the coefficient matrices, while stability and ill–conditioning are seen as critical factors in determining their utility. In particular, the accuracy of an infinite element relies on the choice of the shape functions towards infinity and the order of approximation. On the other hand, infinite elements can be used to discretize the whole exterior domain without truncating it, and from the point of view of open boundaries, they can be seen as a local absorbing boundary condition. In this context, usually there is also an inner conventional finite element mesh close to the object, the choice of the location of the interface between the two meshes being critical to the accuracy properties of a coupled finite/infinite elements discretization.

Our collocation formulation with scaled Laguerre functions tackles the problem from a different perspective. While the shape functions of infinite elements formulations are obtained by the ones of finite elements either by mapping or by multiplication by decay functions, in our approach the equations are directly approximated in the semi–infinite domain out of the artificial boundary. On one hand, this method enjoys spectral accuracy, which is helpful if an appropriate description is sought for the solution in the semi–infinite domain. On the other hand, the use of a small number of base functions (i.e. collocation nodes) would significantly reduce the whole computational cost and, ultimately, yield a more efficient tool for the treatment of open boundary conditions.

5 Coupling finite size and semi-infinite domains

We describe a classical finite–volume method for the numerical approximation of the shallow water equations in a finite domain and show how to attach to this discretization a spectral discretization on a half line, in order to employ the obtained setting as an absorbing boundary condition. To this end, the finite volume discretization is used as an example, being a standard approximation technique for the shallow water equations [22], and we remark that different methods can be employed in the finite domain.
The conservative formulation of shallow water equations reads:

$$\frac{\partial \mathbf{U}}{\partial t} + \frac{\partial \mathbf{F}(\mathbf{U})}{\partial x} = \mathbf{0}, \tag{6}$$

where:

$$\mathbf{U} = \begin{bmatrix} H \\ Hu \end{bmatrix}, \qquad \mathbf{F}(\mathbf{U}) = \begin{bmatrix} Hu \\ Hu^2 + \frac{1}{2}gH^2 \end{bmatrix}.$$

$\mathbf{U}$ is the vector of the conserved quantities (depth and discharge), $\mathbf{F}(\mathbf{U})$ is the flux function.
We want to solve (6) in the spatial and temporal domain $[x_1, x_2] \times [0, T]$. We divide the interval $[x_1, x_2]$ in N_x cells of uniform length Δx, denoted by $[x_{i-\frac{1}{2}}, x_{i+\frac{1}{2}}]$, $i = 1, \ldots, N_x$, the centres of the cells being the points x_i, $i = 1, ..., N_x$.
The numerical solution is approximated by *cell averages* of the solution over grid cells. These averages are then updated at each time step through the fluxes crossing the cell boundary points $x_{i-\frac{1}{2}}$, $x_{i+\frac{1}{2}}$, the *interfaces*.
As for the time discretization, we use a uniform mesh $t^n = n\Delta t$, $n = 0, \ldots, T/\Delta t$ and a fully explicit method. We define $\mathbf{U}_i^n$, the numerical approximation to the cell average at time t^n over the i–th cell, by:

$$\mathbf{U}_i^n \approx \frac{1}{\Delta x} \int_{x_{i-\frac{1}{2}}}^{x_{i+\frac{1}{2}}} \mathbf{U}(x, t^n)\, dx,$$

and the approximation to the flux at the interface $x_{i-\frac{1}{2}}$ by:

$$\mathbf{F}_{i-\frac{1}{2}}^n \approx \frac{1}{\Delta t} \int_{t^n}^{t^{n+1}} \mathbf{F}\left(\mathbf{U}\left(x_{i-\frac{1}{2}}, t\right)\right) dt.$$

$\mathbf{F}_{i-\frac{1}{2}}^n$ is the *numerical flux*. A finite volume method in conservation form reads (see e.g. [21]):

$$\mathbf{U}_i^{n+1} = \mathbf{U}_i^n - \frac{\Delta t}{\Delta x}\left(\mathbf{F}_{i+\frac{1}{2}}^n - \mathbf{F}_{i-\frac{1}{2}}^n\right). \tag{7}$$

An example is the finite volume method obtained by Lax Friedrichs' numerical flux:

$$\mathbf{F}_{i-\frac{1}{2}}^n = \frac{1}{2}\left(\mathbf{F}\left(\mathbf{U}_{i-1}^n\right) + \mathbf{F}\left(\mathbf{U}_i^n\right)\right) - \frac{\Delta x}{2\Delta t}\left(\mathbf{U}_i^n - \mathbf{U}_{i-1}^n\right).$$

We refer to [21] for a detailed discussion on Godunov's method, Roe linearization and its higher–order extensions with slope limiters applied to shallow water equations.
Next, in order to use the spectral semi–infinite discretization described in section 3 as an absorbing layer to extend the finite domain discretization, we need a strategy to couple the two domains, that is, to connect the right endpoint of the finite domain to the left endpoint of the semi–infinite one, the contact point being the *interface*. A representation of the coupling setting is displayed in figure 2.

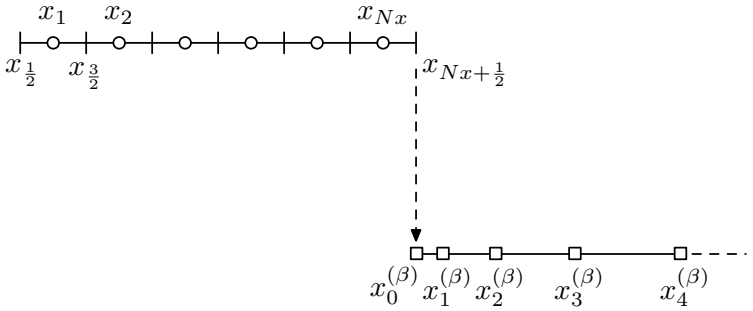

Figure 2: Nodes (circles) and cell interfaces (ticks) of the finite interval discretization, along with the nodes (squares) of the semi–infinite part.

Multidomain discretizations for hyperbolic problems involve suitable conditions on the fluxes or the characteristic variables at the interface between the two domains. For a detailed discussion on the topic we refer to [5, 26]. In our case, we found that a simple condition on continuity of the mass flux is sufficient for the interface to be transparent as waves pass through it. On one hand, this proves to be an effective way to couple the semi–infinite discretization with a flux–based finite volume scheme; on the other hand, this approach enables to use the semi–implicit method in the semi–infinite domain and does not force us to use a characteristic–based numerical scheme, as we should have done when using a classical characteristic coupling. Recalling the discrete formulation (3) of the Neumann boundary condition for the semi–infinite part:

$$(d_\beta)^0 \underline{\mathbf{H}}_N^n \mathbf{u}_N^{n+1} = \left[(D_\beta)_{00} \left(H_N^n u_N^{n+1} \right)_0 + \breve{\mathbf{d}}_\beta \left(\underline{\widehat{\mathbf{H}}}_N^n \widehat{\mathbf{u}}_N^{n+1} \right) \right] = f^{n+1},$$

the coupling is obtained assuming that f^{n+1} is computed from the values of the bounded domain. For simplicity, to obtain this approximation we use a first–order one–sided finite difference formula, i.e. we impose:

$$f^{n+1} = \frac{(hu)^{n+1}(x_{Nx}) - (hu)^{n+1}(x_{Nx-1})}{\Delta x}, \tag{8}$$

where Δx is the finite domain uniform grid spacing. The quantities on the right hand side of (8) result from time advancing the finite volume scheme according to (7).
Dually, the numerical flux at the last interface of the left domain $x_{Nx+1/2}$ is computed taking as right states the depth and discharge values at the

left endpoint $x_0^{(\beta)}$ of the the semi–infinite domain.
Therefore, the solution of the coupled scheme entails the execution of the following algorithm:

For each t^n, $n = 0, \ldots, T/\Delta t - 1$:

1. *Advance the finite volume scheme by* (7)*, having computed* $F^n_{Nx+\frac{1}{2}}$ *assuming a right state:*

$$\mathbf{U}^n_{Nx+1} = \left(h\left(x_0^{(\beta)}\right), h\left(x_0^{(\beta)}\right) u\left(x_0^{(\beta)}\right)\right).$$

2. *Compute:*

$$f^{n+1} = \frac{(hu)^{n+1}(x_{Nx}) - (hu)^{n+1}(x_{Nx-1})}{\Delta x},$$

and replace it in:

$$(d_\beta)^0 \underline{\underline{\mathbf{H}}}^n_N \mathbf{u}^{n+1}_N = \left[(D_\beta)_{00}\left(H^n_N u^{n+1}_N\right)_0 + \breve{\mathbf{d}}_\beta\left(\underline{\underline{\widehat{\mathbf{H}}}}^n_N \widehat{\mathbf{u}}^{n+1}_N\right)\right] = f^{n+1}.$$

3. *Advance the spectral collocation scheme by solving system* (4).

6 Numerical tests

In the sequel we present the results obtained with the numerical schemes described above. First, we deal with the spectral discretization, and test the accuracy of a stand–alone spectral collocation approximation of shallow water equations described in section 3. Next, we validate the coupling approach described in section 5 by matching a semi–infinite spectral discretization with a standard finite volume approximation of the shallow water equations and compare the results with those of a full finite volume approximation, showing that the interface is sufficiently transparent to the the propagation of waves. These results will give motivation for the use of the spectral semi–infinite discretization as an absorbing layer for the approximation of open boundary conditions for waves departing from the finite domain. In particular, we show that a reasonable number of spectral base functions to the right of the artificial interface is sufficient to damp the waves without reflections either at the interface or at infinity.
Given two functions u_N and u defined on Ω, we denote the absolute and relative L^p error of u_N with respect to u by:

$$\mathcal{E}^{abs}_p(u_N) = \|u - u_N\|_p \qquad \forall\, 1 \le p \le \infty$$
$$\mathcal{E}^{rel}_p(u_N) = \frac{\|u - u_N\|_p}{\|u\|_p} \qquad \forall\, 1 \le p \le \infty$$

where:

$$\|u\|_p = \left(\int_\Omega |u|^p\, dx\right)^{1/p} \qquad \forall\, 1 \le p < \infty$$
$$\|u\|_\infty = \sup_{x\in\Omega} |u(x)|.$$

We also denote, for a vector $\mathbf{u} = \{u_j\}_{j=1}^N$:

$$\|\mathbf{u}\|_p = \left(\sum_j |u_j|^p \right)^{1/p} \qquad \forall\, 1 \leq p < \infty$$
$$\|\mathbf{u}\|_\infty = \max_j \left(|u_j| \right).$$

Finally, we denote the global Courant number for a discretization I_j of a spatial interval Ω by:

$$C = \Delta t \max_j \left[\frac{|u_j^n + c_j^n|}{\Delta x_j} \right],$$

where u_j^n is the velocity computed by the numerical scheme at time t^n in the j–th cell, and $c_j^n = \sqrt{gH_j^n}$.

6.1 Validation of the spectral collocation method

The objective of these first set of tests is to validate the use of scaled Laguerre functions to approximate hyperbolic initial boundary–value problems. To this end, we show the results obtained with the spectral collocation discretization of the shallow water equations in a semi–infinite domain. In particular, for simplicity an implicit Euler time discretization is adopted. As for the domain data, setting $\beta = 10^{-3}$ and $N = 100$ internal nodes, one has $x_N^{(\beta)} = 3.77 \cdot 10^5\ m$. We consider homogeneous Neumann boundary condition on the discharge, i.e. expression (2c) with $f = 0$. As initial condition on the free surface elevation, we consider a bell–shaped perturbation:

$$\eta_0(x) = \widetilde{\eta} \exp\left[-\left(\frac{x - x_0}{\sigma} \right)^2 \right], \tag{9}$$

that is, a Gaussian hump of amplitude $\widetilde{\eta}$ centred in $x = x_0$ with a standard deviation σ. The initial velocity is set to zero. Specifically, the hump is centred at $x_0 = 80000\ m$, with $\sigma = 20000\ m$. We solve the shallow water equations with the following data:

$$T = 15000\ s,\ \Delta t = 6\ s,\ \bar{H} = 10\ m,\ \overline{u} = 0\ m/s,\ \widetilde{\eta} = 0.3\ m.$$

The corresponding global Courant number is 1.635. Figure 3 shows the initial depth, figure 4 its evolution under the numerical scheme. The hump splits into two crests propagating at the correct velocity $c = \sqrt{gH}$. When the left crest reaches the left endpoint, it is reflected rightwards. In order to show that the present scheme correctly reproduces the wave propagation process, we report in figure 5 a zoom on the right–going wave, computed by the semi–implicit semi–Lagrangian scheme (solid black line), as well as a reference solution computed by a standard finite-volume solver (dashed red line). Furthermore, the condition numbers of the matrix relative to system (5) for different choices of the number of nodes are displayed in table 1, showing that no conditioning problem arises.

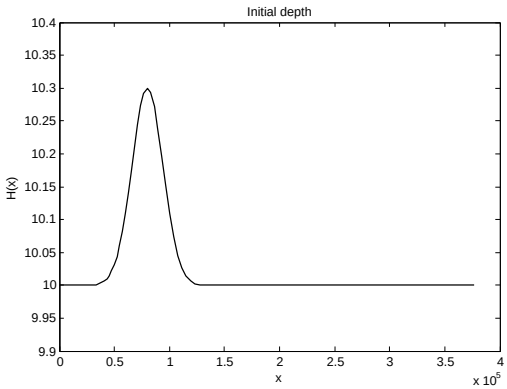

Figure 3: Initial depth for validation of spectral–collocation scheme.

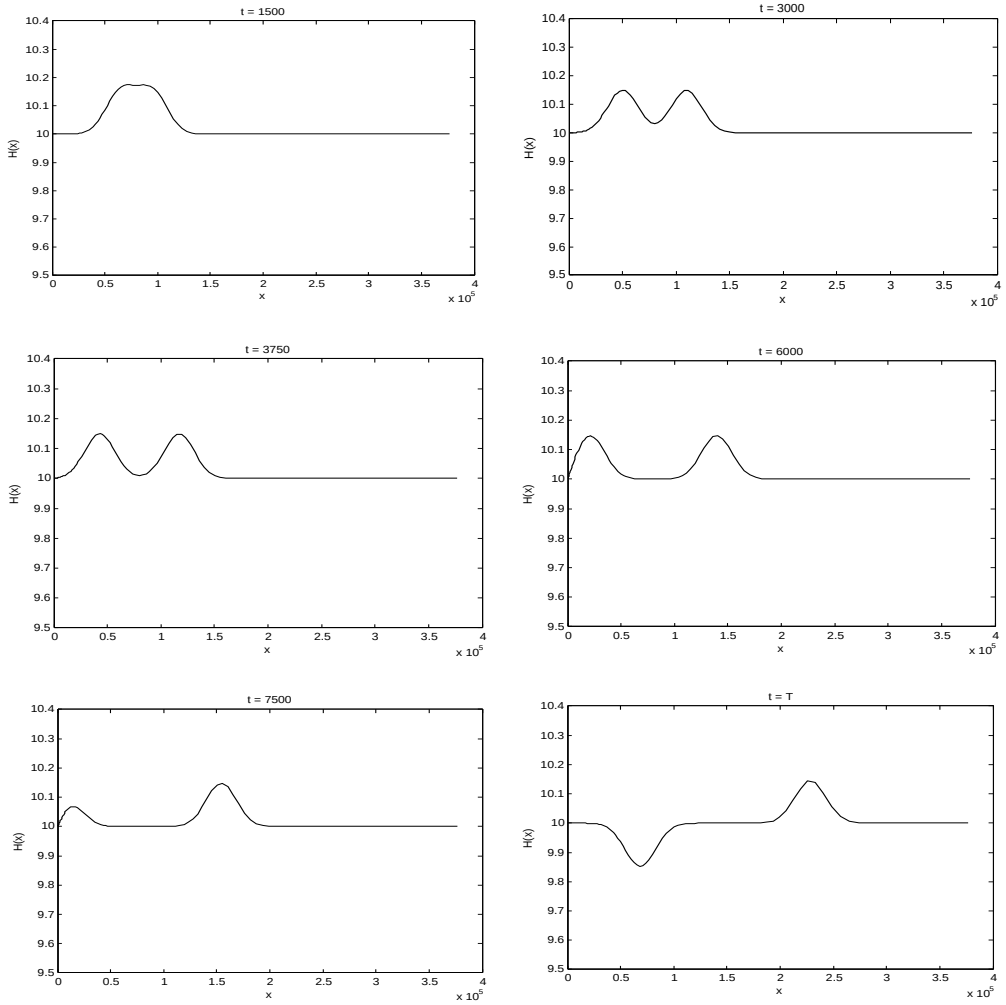

Figure 4: Evolution of an initial Gaussian depth perturbation with implicit Euler–spectral collocation scheme, $C \approx 1.64$, homogeneous Neumann boundary conditions.

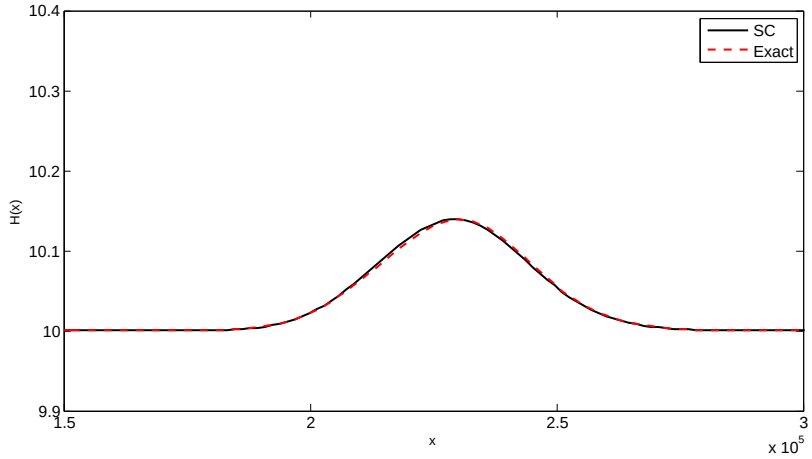

Figure 5: Detail of the comparison of the solution computed by the spectral–collocation method (solid black) with a reference discretization (dashed red)

N	4	8	16	32	64	128	180
K_2	1.008	1.03	1.1	1.39	2.53	7.03	12.88

Table 1: Condition numbers of the matrix of the system (5) for spectral–collocation approximation of shallow water equations, homogeneous Neumann boundary conditions.

Next, in order to use the semi–infinite discretization as an absorbing layer, we consider the shallow water equations with nonzero damping coefficient. In particular, we consider homogeneous Neumann boundary conditions and the following damping function:

$$\gamma(x) = \gamma_D(\Delta\gamma, \alpha, w, L_0, x),$$

where:

$$\gamma(x) = \gamma_D(\Delta\gamma, \alpha, w, L_0, x) := \frac{\Delta\gamma}{1 + \exp\left(\dfrac{\alpha L_0 - x}{\sigma}\right)}.$$

For this test case:

$$L_0 = 4 \cdot 10^5 \ m, \ \alpha = 0.7, \ \Delta\gamma = 0.005, \ w = L_0/2,$$

so that the damping function is centred in $x = 280000$ m (see figure 6). Moreover, now $T = 40000$ s, $\Delta t = 16$ s, so that $C \approx 4.88$. Figure 7 shows the results of the evolution of the initial hump; as in figure 4, the left crest is reflected at the left endpoint, but now the right–going one is damped as expected until all the perturbations are negligible, as can be seen by the plot of the depth at final time.

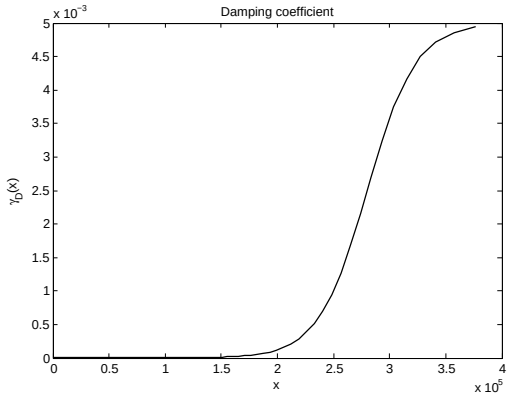

Figure 6: Damping coefficient for spectral–collocation scheme validation.

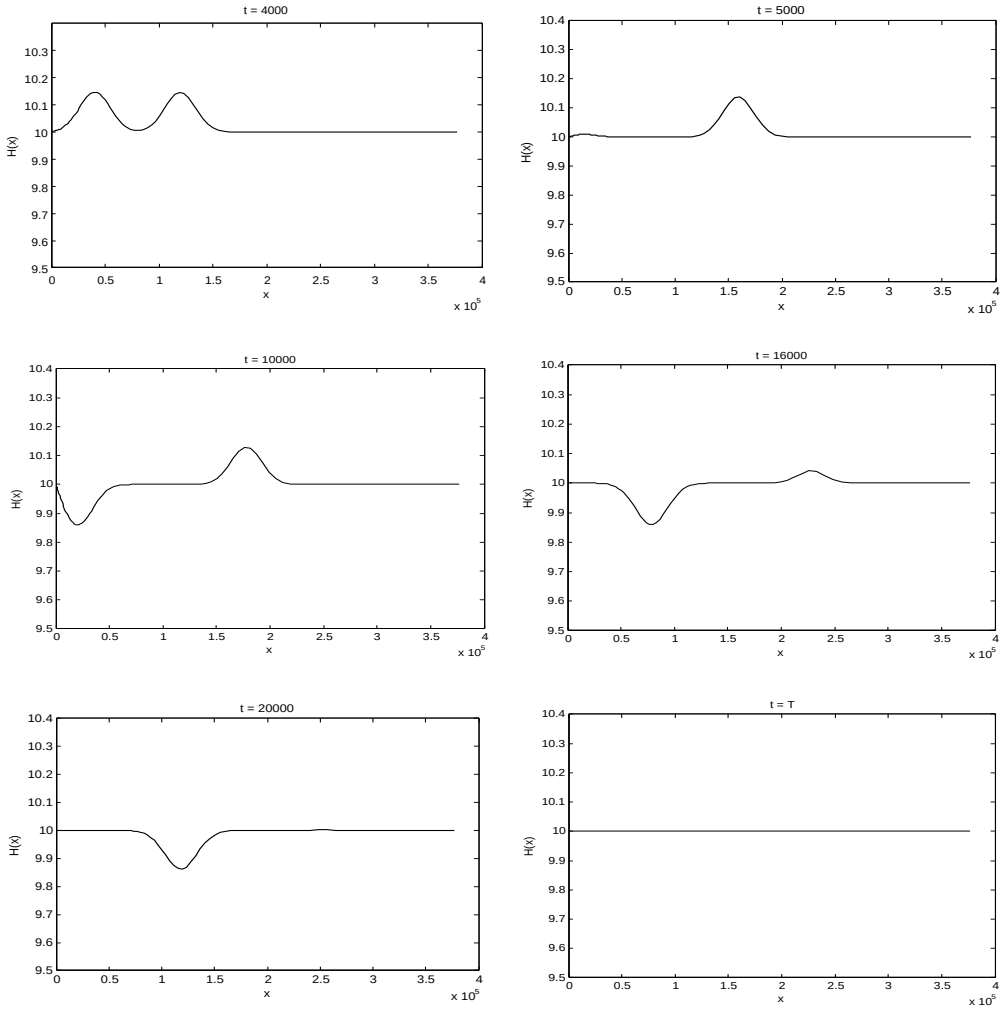

Figure 7: Evolution of an initial Gaussian depth perturbation with implicit Euler–spectral collocation scheme with damping, $C \approx 4.88$, homogeneous Neumann boundary conditions.

6.2 Validation of the coupling approach

To test the accuracy of the coupling strategy described in section 5, we compare the coupled finite/semi–infinite discretization with a stand–alone finite volume approximation. To this end, we consider again the initial condition (9) on free surface elevation for the shallow water model, the initial velocity being again set to zero. We compare the results of a full finite volume approximation with the ones of the coupled finite volume/spectral collocation approximation, considering the full finite volume scheme as the reference solution. We recall that the finite volume approximation is performed on the conservative formulation of the shallow water equations (see above, Eqs. (6) and (7)) with Lax–Friedrichs', Godunov–Roe or minmod slope–limited spatial second order numerical fluxes (see e.g. [21]). As for the spectral part, the spectral collocation scheme described in section 3 is used for space discretization, using cubic interpolation for the reconstruction of the velocity at the foot of the characteristics in the semi–Lagrangian method.

In this setting, the aim is to show that no spurious phenomena occur as a wave travelling in either direction crosses the interface. Indeed, we check that in the finite domain the relative error of the coupled discretization with respect to the full finite volume one is small enough to validate the coupling approach. The lack of spurious phenomena arising from the interface will give a motivation for the use of the spectral semi–infinite discretization as a possible alternative to standard absorbing layers.
We consider the coupled approximation described in section 5, with the following data:

$$\widetilde{\eta} = 1\ m,\ H_N^0 = 10\ m,\ x_{\frac{1}{2}} = 0,\ x_{Nx+\frac{1}{2}} = x_0^{(\beta)} = 10000\ m,$$
$$\beta = 1/400, N_x = 1250,\ N = 180,\ x_N^{(\beta)} = 2.86 \cdot 10^5\ m,$$

where we recall that $x_{\frac{1}{2}}$ is the left endpoint of the finite domain, $x_{Nx+\frac{1}{2}} = x_0^{(\beta)}$ is the interface between the two domains, N_x is the number of cells of the finite volume discretization of the left domain, N is the number of nodes of the spectral semi–infinite collocation approximation, $x_N^{(\beta)}$ is the rightmost spectral node. The parameters must be set up so that the semi–infinite domain grid spacing is of the same order of the finite volume grid spacing at the interface, that is:

$$x_{Nx+\frac{1}{2}} - x_{Nx-\frac{1}{2}} \approx x_1^{(\beta)} - x_0^{(\beta)}.$$

Indeed, several numerical tests (not reported here) show that if the above condition is violated, spurious reflections are more likely to occur at the interface, corrupting the solution in the finite domain.

Test 1

We centre the initial perturbation at $x_0 = 12000\ m$, to the right of the interface. Figure 8 shows the initial depth for two different values of σ.

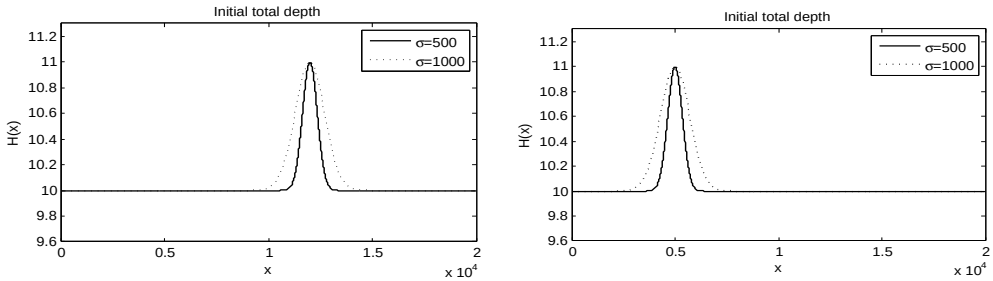

Figure 8: Initial depth perturbations for test 1 (left) and 2 (right).

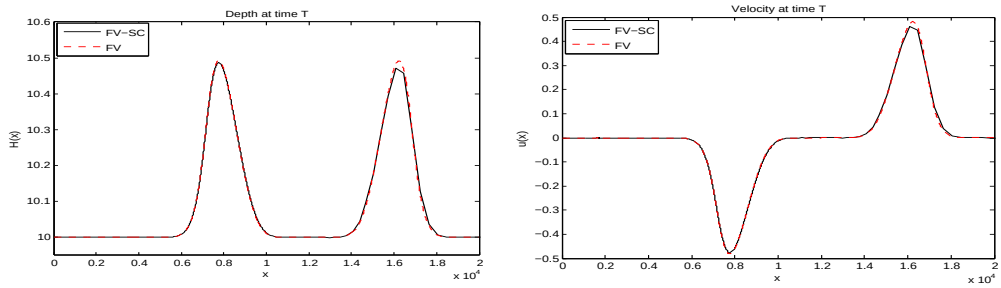

Figure 9: Comparison of coupled (solid black) and full finite volume (dashed red) schemes' computed depth (left) and velocity (right).

Table 2: Test 1 results, $C \approx 0.6$, $\sigma = 500\ m$.

		$\theta = 1$			$\theta = 0.6$		
		LF	GD	SL–MM	LF	GD	SL–MM
$\mathcal{E}_1^{rel}$	$\boldsymbol{\eta}$	1.49E-04	1.33E-04	2.23E-04	2.62E-04	1.92E-04	1.93E-04
	$\mathbf{u}$	0.034	0.03	0.05	0.059	0.044	0.0044
$\mathcal{E}_2^{rel}$	$\boldsymbol{\eta}$	3.19E-04	3.15E-04	4.99E-04	5.74E-04	4.22E-04	4.36E-04
	$\mathbf{u}$	0.027	0.026	0.04	0.0027	0.0027	0.0028
$\mathcal{E}_\infty^{rel}$	$\boldsymbol{\eta}$	0.0012	0.0012	0.0024	0.0021	0.0018	0.0018
	$\mathbf{u}$	0.029	0.027	0.051	3.93E-04	3.47E-04	3.41E-04

Table 3: Test 1 results, $C \approx 0.6$, $\sigma = 1000\ m$.

		$\theta = 1$			$\theta = 0.6$		
		LF	GD	SL–MM	LF	GD	SL–MM
$\mathcal{E}_1^{rel}$	$\boldsymbol{\eta}$	5.9E-05	5.1E-05	6.92E-05	1.09E-04	4.6E-05	2.1E-05
	$\mathbf{u}$	0.0067	0.0058	0.008	0.012	0.005	0.0024
$\mathcal{E}_2^{rel}$	$\boldsymbol{\eta}$	1.07E-04	9.22E-05	1.41E-04	2.02E-04	8.71E-05	4.06E-05
	$\mathbf{u}$	0.0062	0.0053	0.008	6.47E-04	2.79E-04	1.3E-04
$\mathcal{E}_\infty^{rel}$	$\boldsymbol{\eta}$	2.91E-04	2.42E-04	4.54E-04	5.93E-04	2.28E-04	1.26E-04
	$\mathbf{u}$	0.0063	0.0051	0.01	5.55E-05	2.16E-05	1.18E-05

We apply the coupling algorithm described in section 5 until the final time $T = 400\ s$. The initial hump splits into two waves travelling in opposite directions. The left crest crosses the interface and, propagating at the correct velocity $\sqrt{gH} \approx 10\ m/s$, reaches at $t = T$ the point $x \approx 8000\ m$, whereas the right crest symmetrically travels the same length in the positive direction.

The coupled configuration is compared with a full finite volume approximation in a domain 20 km wide with the same initial data. Grid spacing has been suitably chosen so that the first 10 km are covered by the same number of nodes of the finite part of the coupled scheme, i.e. $N_x = 1250$ in the first 10 km. In view of the use of the coupled discretization to simulate open boundary conditions, we want reflections into the finite domain generated at the interface to be minimized. Table 2 shows, for $\sigma = 500\ m$ and $C \approx 0.6$ ($T/\Delta t = 840$) , the L^1, L^2 and L^∞ errors on free surface elevation and velocity in the first 10 km computed by the coupled model relative to the same quantities computed by the full finite volume discretization, taken as reference. We consider different choices (Lax–Friedrichs, Godunov–Roe, minmod slope limited) of the numerical flux for the finite volume approximations, with fully implicit ($\theta = 1$) and semi–implicit ($\theta = 0.6$) time discretizations of the coupled scheme.

Results for the longer wavelength case ($\sigma = 1000\ m$) are reported in table 3, while figure 9 shows comparison of computed final depth and velocity at the final time by the coupled and full finite volume schemes. For this example, we considered $C \approx 0.9$, $\theta = 1$, $\sigma = 1000\ m$ and Lax–Friedrichs flux. For all practical purposes, the solution computed by the coupled formulation approximates well the one computed by the reference method. Further tests with other values of the Courant number, leading to comparable results, are reported in [2]. Relative errors are higher for the shorter wave and for the velocity variable. Nonetheless, on the whole they are all acceptable in an environmental modelling context, cfr. e.g. [29].

Test 2

In this second test we centre the initial perturbation η_0, again with $\widetilde{\eta} = 1\ m$, at $x_0 = 5000\ m$, i.e. in the finite domain, see figure 8. We run the coupled and the full finite volume scheme taking as final time $T = 1000\ s$. At this time, as $c = \sqrt{gH} \approx 10\ m/s$, all the waves are out

of the finite domain, since a transmissive boundary condition is applied at the left endpoint of the finite domain. Therefore, the elevation and velocity variables are expected to be zero in the finite domain. The other parameters are the same as in the previous case. This test aims to check that no spurious waves are generated at the interface. Absolute L^1, L^2 and L^∞ errors for $C \approx 0.3$ ($T/\Delta t = 4200$) are reported in table 4 for $\sigma = 500\ m$, in table 5 for $\sigma = 1000\ m$. L^1 and L^2 errors have been rescaled by the domain length and its square root, respectively, to obtain average values. Further test cases are reported in [2].

Table 4: Test 2 results, $C \approx 0.3$, $\sigma = 500\ m$.

		$\theta = 1$			$\theta = 0.6$		
		LF	GD	SL–MM	LF	GD	SL–MM
$\mathcal{E}_1^{rel}$	$\boldsymbol{\eta}$	7.5E-04	9.4E-04	1.41E-03	8.95E-04	1.25E-03	1.8E-03
	$\mathbf{u}$	7.4E-04	9.3E-04	1.4E-03	8.8E-04	1.24E-03	1.7E-03
$\mathcal{E}_2^{rel}$	$\boldsymbol{\eta}$	3.1E-03	3.9E-03	5.2E-03	3.7E-03	5.7E-03	6.5E-03
	$\mathbf{u}$	3E-03	3.8E-03	5.1E-03	3.7E-03	5.6E-03	6.5E-03
$\mathcal{E}_\infty^{rel}$	$\boldsymbol{\eta}$	0.028	0.032	0.034	0.037	0.256	0.045
	$\mathbf{u}$	0.028	0.032	0.033	0.037	0.257	0.045

Table 5: Test 2 results, $C \approx 0.3$, $\sigma = 1000\ m$.

		$\theta = 1$			$\theta = 0.6$		
		LF	GD	SL–MM	LF	GD	SL–MM
$\mathcal{E}_1^{rel}$	$\boldsymbol{\eta}$	1.7E-05	4.7E-05	6.2E-05	2E-05	6.1E-05	8.2E-05
	$\mathbf{u}$	1.6E-05	4.6E-05	6.2E-05	2E-05	6.1E-05	8.1E-05
$\mathcal{E}_2^{rel}$	$\boldsymbol{\eta}$	1.2E-04	3.3E-04	3.9E-04	1.5E-04	4.4E-04	5.2E-04
	$\mathbf{u}$	1.2E-04	3.3E-04	3.9E-04	1.5E-04	4.3E-04	5.2E-04
$\mathcal{E}_\infty^{rel}$	$\boldsymbol{\eta}$	0.0025	0.0053	0.0053	0.0033	0.007	0.0071
	$\mathbf{u}$	0.0023	0.0052	0.0053	0.0031	0.0069	0.007

6.3 Validation of the efficiency for absorbing boundary conditions

In the previous tests we have validated the coupling strategy by showing that the amplitude of reflected waves at the interface is small, carrying out our analysis in the idealized situation of a high number of nodes. Our ultimate purpose, though, is to use the coupled discretization to implement absorbing layer–type open boundary conditions, and here we present the numerical results obtained in this direction. In our case, the absorbing layer is simulated by a damping reaction coefficient placed in the semi–infinite part. Specifically, we want to show that, on one hand, reducing the number of spectral collocation nodes the coupling strategy does not give rise to numerical instability at the interface, on the other hand, that

waves can be effectively damped in the semi–infinite domain in a finite time interval towards the external solution, that we assume to be zero both for the elevation and the velocity. To this end, we consider again a finite domain of length 10 km and evolve through the interface an initially motionless Gaussian elevation perturbation given by (9), with $\widetilde{\eta} = 1\ m$ and $H_N^0 \equiv 10\ m$. We expect both elevation and velocity to be damped by the the relaxation term which, however, should not produce spurious waves neither in the finite nor in the semi–infinite part. The performance of this new absorbing layer open boundary condition is assessed in terms of maximum values of residual elevation and velocity after the damping.

For simplicity we consider only the case of the implicit Euler method ($\theta = 1$), Lax–Friedrichs flux for the finite volume approximation and linear interpolation for the computation of the characteristics in semi–Lagrangian method. For a decreasing number of nodes, we report the maximum norm of the elevation and velocity vector for the two wavelengths $\sigma = 500\ m$ and $\sigma = 1000\ m$ and two central values $x_{01} = 4000\ m$, $x_{02} = 7000\ m$ for the initial perturbation. Furthermore, to compare results we take $T = 5000\ s$ as a final time. In each test, the grid spacing in the semi–infinite part is set by tuning the value of β; as above, the resulting grid spacing must be of the same order of the finite volume grid spacing at the interface, that is:

$$x_{Nx+\frac{1}{2}} - x_{Nx-\frac{1}{2}} \approx x_1^{(\beta)} - x_0^{(\beta)}.$$

We recall that the damping is modeled by the coefficient:

$$\gamma(x) = \gamma_D(\Delta\gamma, \alpha, w, L_0, x),$$

a sigmoid of width w centred in $x = \alpha L_0$ connecting the values 0 and $\Delta\gamma$. In our case we set $L_0 \approx x_N^{(\beta)}$, and $w = L_0/2$. The value of α is set according to the domain length, in order to let the damping process begin around the point $x_0 = 30000\ m$, which, for the present test, corresponds approximately to $t = T/2$.

N = 40

Setting $L = 800$ ($\beta = 0.00125$), we impose $L_0 \approx x_N^{(\beta)} \approx 1.15 \cdot 10^5\ m$, $\alpha = 0.6$, $N_x = 100$ and $T/\Delta t = 2000$, so that $C \approx 0.3$. Elevation and absolute velocity values are reported in table 6. Residual values are small in both cases, with better results for the shorter wavelength case. Moreover, as expected, a stronger damping entails smaller final values, whereas the initial position of the wave seems not to have a clear influence on the residual elevation and velocity after the damping.

		$\Delta\gamma = 1$		$\Delta\gamma = 2$	
		x_{01}	x_{02}	x_{01}	x_{02}
σ	500	4.6E-03	5.32E-03	2.43E-03	2.73E-03
	1000	7.72E-03	1.10E-02	3.51E-03	5.05E-03

		$\Delta\gamma = 1$		$\Delta\gamma = 2$	
		x_{01}	x_{02}	x_{01}	x_{02}
σ	500	3.39E-03	8.85E-03	1.45E-03	4.23E-03
	1000	8.52E-03	1.33E-02	4.06E-03	6.15E-03

Table 6: Maximum elevation (above) and velocity (below) norm, $N = 40$.

N = 30

Taking again $L = 800$ ($\beta = 0.00125$), we have $L_0 \approx x_N^{(\beta)} \approx 8.48 \cdot 10^4\ m$ and we take $\alpha = 0.65$, $T/\Delta t = 2000$, $N_x = 100$, so that $C \approx 0.25$. Elevation and absolute velocity values are reported in table 7. As before, results are better for the shorter wavelength and for a stronger damping.

		$\Delta\gamma = 1$		$\Delta\gamma = 2$	
		x_{01}	x_{02}	x_{01}	x_{02}
σ	500	6.02E-03	1.24E-02	4.09E-03	8.58E-03
	1000	9.82E-03	1.78E-02	7.33E-03	1.3E-02

		$\Delta\gamma = 1$		$\Delta\gamma = 2$	
		x_{01}	x_{02}	x_{01}	x_{02}
σ	500	6.25E-03	6.56E-03	3.01E-03	3.35E-03
	1000	1.04E-02	1.31E-02	4.94E-03	9.86E-03

Table 7: Maximum elevation (above) and velocity (below) norm, $N = 30$.

N = 20

Choosing again $L = 800$ ($\beta = 0.00125$), we have $L_0 \approx x_N^{(\beta)} \approx 5.47 \cdot 10^4\ m$, $\alpha = 0.7$, and we assume $T/\Delta t = 1200$, $N_x = 55$, so that $C \approx 0.25$. Elevation and absolute velocity values are reported in table 8. As before, results are better for the shorter wave and for a stronger damping, though the coarser resolution in the last part of the semi–infinite domain makes the damping process less effective.

		$\Delta\gamma = 1$		$\Delta\gamma = 2$	
		x_{01}	x_{02}	x_{01}	x_{02}
σ	500	3.87E-03	3.46E-03	1.38E-03	1.77E-03
	1000	8.85E-03	8.08E-03	2.75E-03	4.05E-03

		$\Delta\gamma = 1$		$\Delta\gamma = 2$	
		x_{01}	x_{02}	x_{01}	x_{02}
σ	500	6.26E-03	1.31E-02	4.98E-03	6.66E-03
	1000	9.92E-03	2.19E-02	9.02E-03	1.16E-02

Table 8: Maximum elevation (above) and velocity (below) norm, $N = 20$.

N = 10

In this last test, the parameters are slightly modified because of the very coarse grid in the semi–infinite part. We take $L = 700$ ($\beta = 0.00143$), so that $L_0 \approx x_N^{(\beta)} \approx 2.22 \cdot 10^4$ m and $\alpha = 0.7$, $T/\Delta t = 2500$, $N_x = 60$, so that $C \approx 0.1$. Elevation and absolute velocity values are in table 9. As before, results are better for the shorter wave and for a stronger damping.

		$\Delta\gamma = 1$		$\Delta\gamma = 2$	
		x_{01}	x_{02}	x_{01}	x_{02}
σ	500	2.85E-03	3.81E-03	3.48E-03	2.45E-03
	1000	7.25E-03	6.16E-03	8.64E-03	4.58E-03

		$\Delta\gamma = 1$		$\Delta\gamma = 2$	
		x_{01}	x_{02}	x_{01}	x_{02}
σ	500	4.7E-03	1.89E-03	3.59E-03	2.16E-03
	1000	1.18E-02	4.31E-03	1.05E-03	3.54E-03

Table 9: Maximum elevation (above) and velocity (below) norm, $N = 10$.

These results on the use of the semi–infinite discretization as an absorbing layer, especially in the case of few nodes, will make possible an extensive comparison with currently used absorbing layers, see e.g. [20, 24]. Here we only remark that standard layers are very thin with respect to the finite domain length, whereas our scaled approach would enable to represent a larger semi–infinite part approximately at the same computational cost, e.g. employing the same number of nodes.

7 Conclusions and future work

In this work we have introduced a numerical method based on Laguerre functions expansions for the approximation of wave propagation problems on semi–infinite domains. In particular, a semi–implicit, semi–Lagrangian discretization has been developed for the one dimensional shallow water equations on semi–infinite domains, along with a coupling approach based

on imposing continuity of mass fluxes at the interface between the bounded and unbounded domain. The semi–implicit, semi–Lagrangian approach has been chosen because of its well known efficiency and accuracy features and because a large number of environmental models use these time discretization techniques. On the other hand, an explicit finite volume discretization has been considered for the finite size domain. Furthermore, by coupling discretizations on domains of finite size to Laguerre spectral methods employing a relatively small number of nodes, an efficient approach to absorbing boundary conditions has been achieved, that allows to account for large absorbing regions at a relatively low computational cost.

A number of numerical tests has been carried out. Firstly, the pseudo–spectral, semi–implicit, semi–Lagrangian discretization on semi–infinite domains has been validated. Moreover, we have shown that spurious reflections due to the proposed coupling approach have very small amplitude and allow to use the method, at least for environmental applications, with no substantial loss of accuracy with respect to single domain discretizations. Next, absorbing boundary conditions have been validated, as implemented in the context of the coupled finite volume/pseudo–spectral model. Numerical simulations have shown that a relatively small number of Laguerre base functions is sufficient to reach the accuracy necessary for practical implementations of open boundary conditions, along with an accurate treatment of the solution behaviour at infinity.

The obtained results appear to confirm that this approach to absorbing layer boundary conditions is advantageous for a number of reasons. It is therefore of interest to consider various natural extensions of the present work, in order to exploit the proposed technique in practical applications.

First, the semi–implicit, semi–Lagrangian pseudo–spectral method on semi–infinite domains can be coupled to different discretizations on the finite size domain; in particular, efficient and commonly used semi–implicit, semi–Lagrangian techniques could be considered in the finite domain, based on either a finite difference or finite element spatial discretization.

Next, two dimensional discretizations of the shallow water equations can be developed, in which a semi–infinite strip is discretized using Laguerre basis functions in the x direction and some other discretization approach in the y direction. For example, tensor product–based multi–dimensional polynomial spaces as in [35] could be employed, or, more simply, finite difference or finite volume discretizations could be used. This would naturally lead to a comparison with the results in [20, 24] on two dimensional test cases.

Finally, coupling two dimensional vertical strips to vertical slice atmospheric models could be considered, see e.g. [3, 13], for the purpose of assessing the effectiveness of this approach in the case of vertically propagating gravity waves. The main target of this further development would be the comparison of the standard absorbing layer approaches (see e.g. [17]) to those built following the ideas proposed in this work. For these numerical models, the extension of the necessary upper absorbing layer is known to increase with the increase in horizontal resolution, thus leading to an extra computational cost that can be especially high for models employing height based coordinates, such as many high resolution numerical weather predic-

tion models. Hence, it would be interesting to assess whether a substantial decrease of the computational cost for these models can be achieved by extending the techniques proposed in this work.

Acknowledgements

This work is a summary of the Master Thesis in Mathematical Engineering prepared by T.Benacchio under the supervision of L. Bonaventura. Useful discussions with A.Quarteroni and constructive critical remarks by F.X.Giraldo are kindly acknowledged.

References

[1] R.J. Astley. Infinite elements for wave problems: a review of current formulations and an assessment of accuracy. *International Journal for Numerical Methods in Engineering*, 49(7):951–976, 2000.

[2] T. Benacchio. Spectral collocation methods on semi–infinite domains and application to open boundary conditions. Master's thesis, Politecnico di Milano, 2010. Available at: `mox.polimi.it/it/progetti/pubblicazioni/tesi/benacchio.pdf`.

[3] L. Bonaventura. A Semi–implicit Semi–Lagrangian Scheme Using the Height Coordinate for a Nonhydrostatic and Fully Elastic Model of Atmospheric Flows. *Journal of Computational Physics*, 158(2):186–213, 2000.

[4] C. Canuto, M. Y. Hussaini, A. Quarteroni, and T. A. Zang. *Spectral Methods. Fundamentals in Single Domains.* Springer–Verlag, Berlin Heidelberg, 2006.

[5] C. Canuto, M. Y. Hussaini, A. Quarteroni, and T. A. Zang. *Spectral Methods. Evolution to Complex Domains and Applications to Fluid Dynamics.* Springer–Verlag, Berlin Heidelberg, 2007.

[6] V. Casulli. Semi–implicit Finite Difference Methods for the Two–Dimensional Shallow Water Equations. *Journal of Computational Physics*, 86:56–74, 1990.

[7] A. Decoene, L. Bonaventura, E. Miglio, and F. Saleri. Asymptotic derivation of the section averaged shallow water equations for natural river hydraulics. *Mathematical Models and Methods in Applied Sciences*, 19:387–417, 2009.

[8] D.R. Durran and J.B. Klemp. A Compressible Model for the Simulation of Moist Mountain Waves. *Monthly Weather Review*, 111:2341–2361, 1983.

[9] B. Engquist and A. Majda. Absorbing boundary conditions for numerical simulation of waves. *Mathematics of Computation*, 31(139):629–651, 1977.

[10] P.E. Francis. The possible use of Laguerre polynomials for representing the vertical structure of numerical models of the atmosphere. *Quarterly Journal of the Royal Meteorological Society*, 98:662–667, 1972.

[11] K. Gerdes. A review of infinite element methods for exterior Helmholtz problems. *Journal of Computational Acoustics*, 8(1):43–62, 2000.

[12] M.A. Giorgetta, E. Manzini, E. Roeckner, M. Esch, and L. Bengtsson. Cilmatology and forcing of the quasi–biennal oscillation in the MAECHAM5 model. *Journal of Climate*, 19(16):3882–3901, 2006.

[13] F.X. Giraldo and M. Restelli. High–order semi–implicit time–integrators of a triangular discontinuous Galerkin oceanic shallow water model. *International Journal for Numerical Methods in Fluids*, 63(9):1077–1102, 2010.

[14] D. Givoli. Computational Absorbing Boundaries. In S. Marburg and B. Nolte, editors, *Computational Acoustics of Noise Propagation in Fluids – Finite and Boundary Element Methods*. Springer Berlin Heidelberg, 2008.

[15] T. Horinouchi, S. Pawson, K. Shibata, U. Langematz, E. Manzini, M.A. Giorgetta, F. Sassi, R.J. Wilson, K. Hamilton, J. De Grandpré, and A.A. Scaife. Tropical cumulus convection and upward–propagating waves in middle–atmospheric GCMs. *Journal of the Atmospheric Sciences*, 60(22):2765–2782, 2003.

[16] M. Israeli and S.A. Orszag. Approximation of Radiation Boundary Conditions. *Journal of Computational Physics*, 41:115–135, 1981.

[17] J.B. Klemp, J. Dudhia, and A.D. Hassiotis. An Upper Gravity–Wave Absorbing Layer for NWP Applications. *Monthly Weather Review*, 136(10):3987–4004, 2008.

[18] J.B. Klemp and D.R. Durran. An Upper Boundary Condition Permitting Internal Gravity Wave Radiation in Numerical Mesoscale Models. *Monthly Weather Review*, 111:430–444, 1983.

[19] J.B. Klemp and D.K. Lilly. Numerical Simulation of Hydrostatic Mountain Waves. *Journal of the Atmospheric Sciences*, 35:78–107, 1978.

[20] J.W. Lavelle and W.C. Thacker. A pretty good sponge: Dealing with open boundaries in limited–area ocean models. *Ocean Modelling*, 20(3):270–292, 2008.

[21] R.J. LeVeque. *Finite volume methods for hyperbolic problems*, volume 31 of *Cambridge texts in applied mathematics*. Cambridge University Press, Cambridge, 2002.

[22] R.J. LeVeque and D.L. George. High–resolution finite volume methods for the shallow water equations with bathymetry and dry states. In P. L.-F. Liu, H. Yeh, and C. Synolakis, editors, *Advanced numerical models for simulating tsunami waves and runup*, volume 10 of *Advances in coastal and ocean engineering*. World Scientific, 2008.

[23] A. McDonald. Transparent Boundary Conditions for the Shallow–Water Equations: Testing in a Nested Environment. *Monthly Weather Review*, 131:698–705, 2003.

[24] A. Modave, É. Deleersnijder, and É.J.M. Delhez. On the parameters of absorbing layers for shallow water models. *Ocean Dynamics*, 60:65–79, 2010.

[25] I.M. Navon, B. Neta, and M. Y. Hussaini. A perfectly matched layer approach to the linearized shallow water equations models. *Monthly Weather Review*, 132(6):1369–1378, 2004.

[26] A. Quarteroni. Domain decomposition methods for systems of conservation laws; spectral collocation approximations. *SIAM Journal on Scientific and Statistical Computing*, 11(6):1029–1052, 1990.

[27] A. Quarteroni, R. Sacco, and F. Saleri. *Numerical Mathematics*. Springer, Berlin Heidelberg, second edition, 2007.

[28] P.J. Rasch. Toward atmospheres without tops: Absorbing upper boundary conditions for numerical models. *Quarterly Journal of the Royal Meteorological Society*, 112:1195–1218, 1986.

[29] G. Rosatti, D. Cesari, and L. Bonaventura. Semi–implicit, semi–Lagrangian modelling for environmental problems on staggered Cartesian grids with cut cells. *Journal of Computational Physics*, 204(1):353–377, 2005.

[30] J. Shen. Stable and efficient spectral methods in unbounded domains using Laguerre functions. *SIAM Journal on Numerical Analysis*, 38:1113–1133, 2001.

[31] J. Shen and T. Tang. *Spectral and high order methods with applications*. Science Press, Beijing, 2006.

[32] J. Shen and L.-L. Wang. Some recent advances on spectral methods for unbounded domains. *Communications in Computational Physics*, 5:195–241, 2009.

[33] A. Staniforth and J. Côté. Semi–Lagrangian integration schemes for atmospheric models–a review. *Monthly Weather Review*, 119(9):2206–2231, 1991.

[34] Z.-Q. Wang, B.-Y. Guo, and Y.-N. Wu. Pseudospectral method using generalized Laguerre functions for singular problems on unbounded domains. *Discrete and Continuous Dynamical Systems Series B*, 11(4):1019–1038, 2009.

[35] Q. Zhuang, J. Shen, and C. Xu. A coupled Legendre–Laguerre spectral–element method for the Navier–Stokes equations in unbounded domains. *Journal of Scientific Computing*, 42(1):1–22, 2010.

MOX Technical Reports, last issues

Dipartimento di Matematica "F. Brioschi",
Politecnico di Milano, Via Bonardi 9 - 20133 Milano (Italy)

33/2011 Antonietti, P.F.; Beirao da Veiga, L.; Lovadina, C.; Verani, M.
Hierarchical a posteriori error estimators for the mimetic discretization of elliptic problems

32/2011 Aletti, G; Ghiglietti, A; Paganoni, A.
A modified randomly reinforced urn design

34/2011 Benacchio, T.; Bonaventura, L.
A spectral collocation method for the one dimensional shallow water equations on semi-infinite domains

31/2011 Astorino, M.; Becerra Sagredo, J.; Quarteroni, A.
A modular lattice Boltzmann solver for GPU computing processors

30/2011 Nobile, F.; Pozzoli, M.; Vergara, C.
Time accurate partitioned algorithms for the solution of fluid-structure interaction problems in haemodynamics

29/2011 Morin, P.; Nochetto, R.H.; Pauletti, S.; Verani, M.
AFEM for Shape Optimization

28/2011 Pischiutta, M.; Formaggia, L.; Nobile, F.
Mathematical modelling for the evolution of aeolian dunes formed by a mixture of sands: entrainment-deposition formulation

27/2011 Antonietti, P.F.; Bigoni, N.; Verani, M.
A Mimetic Discretization of Elliptic Control Problems

26/2011 Secchi, P.; Vantini, S.; Vitelli, V.
Bagging Voronoi classifiers for clustering spatial functional data

25/2011 de Luca, M.; Ambrosi, D.; Robertson, A.M.; Veneziani, A.; Quarteroni, A.
Finite element analysis for a multi-mechanism damage model of cerebral arterial tissue